Gamma-ray emission from molecular clouds illuminated by local young massive stellar clusters and detection prospects with current and next generation instruments

S. Celli,[a,b,c,*] A. Specovius,[d] A. Mitchell,[d] G. Morlino[e] and S. Menchiari[e,f]

[a] *Sapienza Università di Roma,*
Piazzale Aldo Moro 5, 00185, Rome, Italy

[b] *Istituto Nazionale di Fisica Nucleare, Sezione di Roma,*
Piazzale Aldo Moro 5, 00185, Rome, Italy

[c] *Istituto Nazionale di Astrofisica, Osservatorio Astronomico di Roma,*
Monte Porzio Catone, 00136, Rome, Italy

[d] *Friedrich-Alexander Universität Erlangen-Nürnberg, Erlangen Centre for Astroparticle Physics,*
Nikolaus-Fiebiger-Str. 2, 91058 Erlangen, Germany

[e] *Istituto Nazionale di Astrofisica, Osservatorio Astrofisico di Arcetri,*
L.go E. Fermi 5, Firenze, Italy

[f] *INFN - Sezione di Pisa, Edificio C - Polo Fibonacci Largo B. Pontecorvo 3, 56127 Pisa, Italy*

E-mail: silvia.celli@roma1.infn.it

Cosmic ray acceleration up to PeV energies has been suggested to take place in massive and young stellar clusters. The formation of a strong termination shock sustained by the collective action of stellar winds in a compact cluster offers a promising location where efficient particle acceleration might take place. The subsequent hadronic interactions of these particles result into gamma-ray production: in particular, if dense clouds are located within and around clusters, enhanced emission is expected. Within a scenario of particle acceleration at the cluster wind termination shock, we compute the emerging gamma-ray signal from molecular clouds illuminated by stellar clusters within the Milky Way. For this purpose, we adopt the Miville-Deschenes cloud catalog based on the Dame CO survey and astrometric observations of stellar clusters by GAIA. We further evaluate detection prospects of the gamma-ray flux with the Cherenkov Telescope Array (CTA) and the Large High Altitude Air Shower Observatory (LHAASO).

*Speaker

PoS(ICRC2023)775

1. Introduction

In the quest for the origin of Galactic Cosmic Rays (GCRs) in the knee region, namely at energies around 10^{15} eV, Young and Massive Stellar Clusters (YMSCs) have been suggested as alternative candidate sources to SuperNova Remnants (SNRs). These continuous accelerators might in fact provide, during a lifetime of several million years, comparable energetics with respect to SNR outputs: in fact, in order to sustain an average wind luminosity of 3×10^{37} erg/s for 10^6 yr, an energy injection of $\simeq 10^{51}$ erg is needed, similarly to the kinetic energy release of SuperNova (SN) explosions. Besides energetic considerations, acceleration of particles from the wind of massive stars appears to be a necessary component to explain the $^{22}Ne/^{20}Ne$ anomaly in CR composition [1]: the enhancement observed with respect to Solar abundances requires acceleration from a carbon-enriched medium rather than from the standard interstellar medium (ISM), e.g. from the wind of Wolf-Rayet stars. The relative contribution of these different source populations, SNRs and YMSCs, to the observed CRs is yet to be clarified, as well as their role across energy and in particular in the region across the *knee* around few PeVs.

Stellar Clusters (SCs) belonging to the disk of the Galaxy, usually referred to as open clusters, consist of homogeneous groups of stars with the same age and initial chemical composition: as such, they constitute ideal laboratories for studying stellar formation and evolution. YMSCs have recently been detected in very-high-energy (VHE) gamma rays [2] with the Imaging Atmospheric Cherenkov Telescope (IACT) H.E.S.S.: its accurate morphological measurements have allowed to infer the spatial distribution of accelerated particles in the surroundings of several Galactic clusters, all consistent with a $1/r$ profiles, possibly induced by diffusion from a central continuous injector. The Cygnus cocoon has even been observed at the highest energies ever reached by gamma-ray astronomy: a 1.4 PeV photon was detected from LHAASO [21], thus probing the capabilities of stellar clusters as PeV-particle accelerators (i.e. PeVatrons, and perhaps even superPeVatrons).

The exact location where particle acceleration takes place in YMSCs is object of active debate in the community, perhaps even depending on the specifics of each cluster. For compact systems, the so-called Wind Termination Shock (WTS) [4] is expected to be strong enough to enable particle acceleration at such extreme energies [5]. Alternatively, stochastic acceleration might be driven in the highly turbulent environment of the cluster, particularly in its core [6], further amplified once SN explosions start to occur [7]. In this work, we will consider only acceleration at the cluster WTS, which is most likely the dominant source of energy during the first few million years of the cluster evolution, namely before SNe explode. The WTS acceleration model under investigation is hence described in Sec. 2, where it is also applied to a sample of YMSC selected from the Gaia survey [8], the most sensitive compilation of open clusters of the Milky Way to date. The radiative signatures induced by the energized particles in nearby dense gas targets [9] are further considered in Sec. 3, where the most accurate catalog of Galactic molecular clouds [10] available is adopted for compiling a list of candidate cluster-cloud systems and evaluating the impact of hadronic collisions in such illuminated clouds. The resulting gamma-ray emissions from these pairs are shown in Sec. 4 and compared to the sensitivity of ground-based gamma-ray instruments, both the operative extensive air shower array LHAASO and the future IACT Cherenkov Telescope Array (CTA), to quantify their detection prospects. Finally, conclusions are drawn in Sec. 5.

2. Particle acceleration at YMSC wind termination shock

Massive stars progressively lose part of the stellar envelope during their evolution through winds driven by the high radiation pressure. Stellar associations can form a collective wind, that is launched together with a forward and a reverse shock. The former is a mild shock compressing the ISM, with a modest efficiency in particle acceleration. The latter, also known as WTS, is a shock sustained by the ram pressure of the wind, whose position can be found by equating the bubble thermal pressure to the wind ram pressure. The stellar cluster is named *compact* if its WTS position R_s is beyond the cluster radius R_c: for compact clusters, the WTS is strong with a typical Mach number of 5-10 [5], hence in principle, effective in accelerating particles. Inside the wind blown bubble, the competition between diffusion and advection determines the particle transport. Following the scheme depicted in Fig. 3(a), we here consider three different diffusion coefficients in the bubble region, namely D_1 in the cold wind, D_2 in the shocked wind and D_3 in the ISM. For the plasma velocity profile, a constant speed u_1 is assumed between R_c and R_s, a wind-like profile $u_2(R_s/r)^2$ between R_s and the bubble radius R_b, and null speed outside. The general solution of the 1D transport equation in a spherical geometry is obtained in [4], with two boundary conditions: at far distances the particle distribution function $f(p)$ matches the average Galactic one $f_{\mathrm{Gal}}(p)$, while at the center of the bubble the net flux is null. Outside of the bubble, the particle density as a function of position r and momentum p reads as

$$f(r > R_b, p) = f_b(p)\frac{R_b}{r} + f_{\mathrm{Gal}}(p)\left(1 - \frac{R_b}{r}\right), \quad (1)$$

while at the bubble radius

$$f_b(p) = \frac{f_s(p)\exp^{\alpha(R_b,p)} + f_{\mathrm{Gal}}\beta(\exp^{\alpha(R_b,p)} - 1)}{1 + \beta(\exp^{\alpha(R_b,p)} - 1)}, \quad (2)$$

where $\alpha(r, p) = u_2 R_s(1 - R_s/r)/D_2(p)$ and $\beta(p) = D_3(p)R_b/(u_2 R_s^2)$. The solution at the WTS reads

$$f_s(p) = \frac{3\xi_{\mathrm{cr}} n_1 u_1^2}{4\pi\Lambda_p(m_p c)^3 c^2}\left(\frac{p}{m_p c}\right)^{-s}\exp^{-\Gamma(p)}, \quad (3)$$

ξ_{cr} being the CR acceleration efficiency in terms of the wind ram pressure $m_p n_1 u_1$, n_1 the wind numerical density, m_p the proton mass, c the speed of light in a vacuum, $s = 4$ the spectral slope of acceleration, and Λ_p a normalization constant. The full solution in Eq. (3) can be approximated by fitting the pure exponential part with the following analytical expression

Figure 1: A schematic illustration of gas clouds illuminated by the particle flux accelerated at a cluster WTS.

$$\exp^{-\Gamma(p)} = (1 + A(p/p_m)^b)\exp^{-k(p/p_m)^c}. \quad (4)$$

We derive $k = 12.52$, $A = 5$, $b = 0.449$ and $c = 0.0643$ for a Kraichnan-like diffusion coefficient, i.e. $D_1 = \frac{v}{3}r_L^{1/3}L_c^{2/3} \equiv k_1 p^{\delta_1}$ with $\delta_1 = 0.5$, v being the particle velocity, r_L its Larmor radius. The coherence length of the magnetic field is assumed $L_c \simeq 2$ pc, comparable to the typical size

of stellar cluster cores. Finally, the *nominal* maximum momentum p_m can be obtained from the condition $D_1 = u_1 R_s$. Lastly, the solution in the cold (upstream) wind reads as

$$f(r < R_s, p) = f_s(p) \exp^{-u_1(R_s - r)/D_1} . \tag{5}$$

Defining the cluster age t, its mass loss rate $\dot{M}_\text{c}$, its wind speed $v_\text{w,c}$ and its wind luminosity $L_\text{w,c} = \frac{1}{2}\dot{M}_\text{c}v_\text{w,c}^2$, as well as the ISM mass density ρ_3, we obtain the bubble and WTS radii by using the adiabatic solution [11], which read

$$R_s(t) = 48.6 \left(\frac{\rho_3}{\text{cm}^{-3}}\right)^{-0.3} \left(\frac{\dot{M}_\text{c}}{10^{-4}\text{M}_\odot\text{yr}^{-1}}\right)^{0.3} \left(\frac{v_\text{w,c}}{1000\,\text{km s}^{-1}}\right)^{0.1} \left(\frac{t}{10\,\text{Myr}}\right)^{0.4} \text{pc} \tag{6}$$

$$R_b(t) = 174 \left(\frac{\rho_3}{\text{cm}^{-3}}\right)^{-0.2} \left(\frac{L_\text{w,c}}{10^{37}\,\text{erg s}^{-1}}\right)^{0.2} \left(\frac{t}{10\,\text{Myr}}\right)^{0.6} \text{pc} . \tag{7}$$

Because stellar clusters are found in the same ISM regions where they are formed, namely Giant Molecular Clouds (GMCs), we here consider an external density of $\rho_3 = 10$ protons/cm^3.

2.1 The stellar cluster sample

The Gaia space mission has allowed more than a billion stars in our Galaxy to be characterised with astrometry at the sub-milliarcsecond level. The application of advanced classification algorithms, based on machine learning techniques, to its second Data Release (so-called DR2) has resulted in the identification of a large and homogeneous sample of clusters, consisting of 1857 objects [8]. Despite this catalog not corresponding to the latest available data release, it contains the most precise information to date concerning cluster members and their physical parameters, namely number and magnitude of individual stars. These are crucial ingredients of the particle acceleration model presented above, particularly in the evaluation of the luminosity of the collective wind and therefore in quantifying the energy channeled into accelerated particles. We further complement this cluster sample by including SCs identified by the Milky Way Stellar Cluster (MWSC) catalog [12]: by merging the two catalogs, we obtained 3865 clusters.

As the acceleration model under investigation relies on the effectiveness of WTSs, which have been shown to be energetically dominant during the early evolution of the stellar cluster [13], we applied a selection criterion to the initial cluster sample by keeping only those younger than 30 Myr. This cut reduced the number of clusters considered to 390, all of which are observed by Gaia. For each cluster in the selected sample, we first evaluate individual cluster masses by assuming a Kroupa-like stellar mass function dN/dM [14], normalized to reproduce the number of stars observed by Gaia in its magnitude range. Because of the intrinsic limitations of this mass estimation procedure, strongly relying on the capabilities of single star identification, our result should rather be interpreted as a lower bound to the actual cluster mass. For the determination of the mass range where stars are detected by Gaia, we consider the minimum and maximum magnitude of the stars belonging to each cluster, correct them for G-band extinction, and relate the corrected magnitudes to stellar masses assuming main sequence evolution. As the correction for G-band extinction is based on the measured stellar effective temperature, the lack of this parameter in three clusters of the sample (IC2948, NGC1333 and Pismis16) reduces clusters the size of the final cluster sample to 387. After normalizing each cluster of such a sample, we compute the expected cluster mass M_c by integrating

(a)   (b)
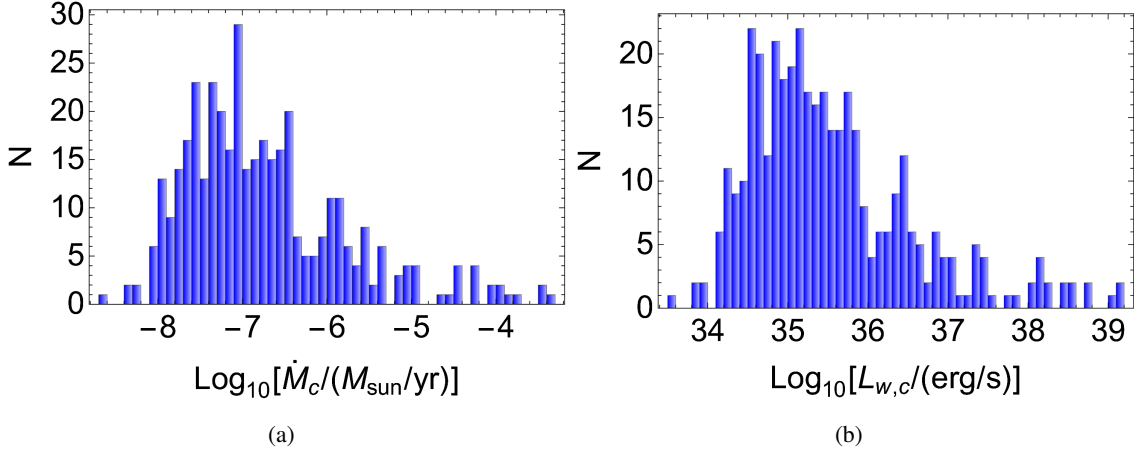
Figure 2: Distribution of wind mass loss rates (a) and luminosities (b) of the selected young clusters.

the mass function between $M_{min} = 0.01\,\mathrm{M}_\odot$ and M_{max}, the latter being whichever value is lower between the maximum stellar mass observed in the Galaxy, $150\,M_\odot$, and the maximum stellar mass allowed at the cluster age by stellar evolution. The stellar cluster mass loss rate $\dot{M}_c$ is then simply obtained by summing the wind mass loss rates from all its stars, while the cluster wind luminosity $L_{w,c}$ is computed by assuming momentum conservation, namely

$$\dot{M}_c v_{w,c} = \int_{M_{min}}^{M_{max}} \frac{dN}{dM} \dot{M}_s(M) v_{w,s}(M) dM \ . \tag{8}$$

The resulting mass distribution of selected clusters has a median value of $442 M_\odot$. Their mass loss rate and wind luminosity distributions are also shown in Figs. 2(a) and 2(b), with median values of $10^{-7}\,M_\odot$/yr and 2×10^{35} erg/s, respectively. With such cluster parameters, we proceed to the calculation of the steady-state CR distribution: further details about this computation are provided in [15]. We here proceed to the investigation of the accelerated particle density impacting off nearby molecular clouds, offering the best conditions for enhanced hadronic interactions, particularly if located around the cluster WTS where the density of accelerated particles is maximum.

3. Enhanced gamma-ray hadronic emission from illuminated molecular clouds

Molecular clouds located in close proximity of a particle accelerator emit non-thermal radiation as a result of hadronic collisions among its dense gas and the injected particles [9, 24], the so-called proton-proton (pp) interactions, particularly at locations where the energy density of such particles is higher. To identify suitable target material in the vicinity of the selected SCs, we adopt the molecular cloud catalogue compiled by [10] (version 3) based on the CO survey [16], containing 9710 clouds. It is the most complete molecular cloud catalog available to date, reporting information about positions in the Galactic Plane, angular sizes, kinematic distances and masses of each cloud, enabling in most of the cases the evaluation of their intrinsic properties, e.g. physical size and average density. We only include in our analysis clouds with a reasonable distance estimate, as well as excluding clouds with density below 10 protons/cm^3, as they would not provide a significant gas
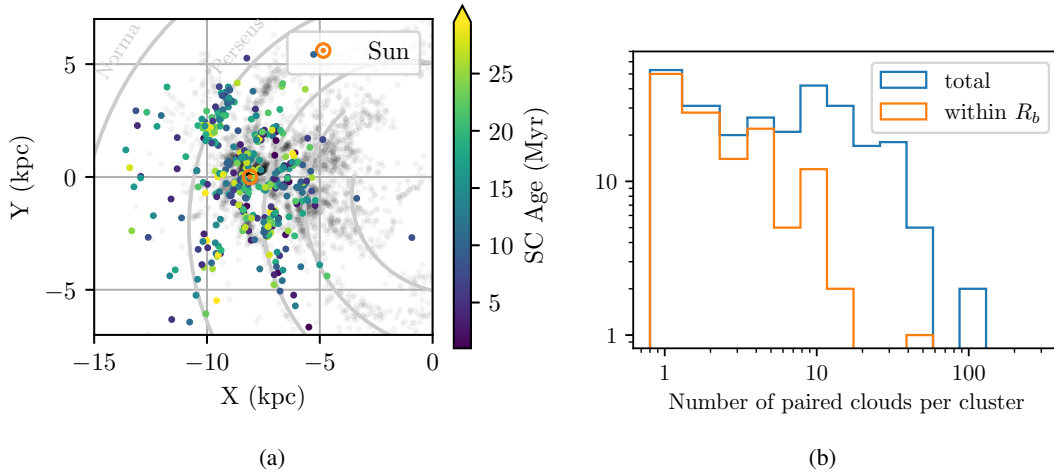
Figure 3: (a) Position in the Galactic Plane of molecular clouds (grey dots) from [10] and selected SCs (colored dots) from [8], overlaid to the Milky Way spiral arms. (b) Number of paired clouds per SC.

enhancement with respect to the local ISM in the cloud surroundings. With these selection criteria, we are left with 4423 clouds as targets for hadronic collisions from the particle flux accelerated at the stellar cluster WTSs. A visual representation of the location in the Galactic Plane of both clusters and clouds is provided in Fig. 3(a), indicating that the known Galactic YMSC population is only locally complete: the median distance value of the selected cluster sample is 2.3 kpc.

3.1 Cluster-cloud pairings

To match each selected cluster with nearby clouds, we consider possible pairings with all the clouds located at distances between the WTS radius and twice the bubble radius. In fact, as the particle density rapidly drops at radial distances beyond the bubble radius (see Eq. 1), clouds located at much larger distances will not be suitable targets for pp interactions due to the reduced incident particle flux. Since position and distance information is available for both the clouds and clusters, a 3D matching is performed under the assumption of spherical symmetry for both the clouds and the wind-blown bubbles around stellar clusters. The number of resulting pairs is shown in Fig. 3(b), with different histograms representing cases where the pairing is obtained with a cloud located inside or outside of the respective cluster bubble: we obtain a total of 2658 pairs, with 1233 distinct clouds participating, meaning that each cluster is associated to more than one cloud on average. For the paired clouds, the median density is ~ 55 protons/cm^3, while their angular diameter is $0.7°$.

4. Gamma rays from hadronic interactions and detection prospects with current and future ground-based gamma-ray instruments

Hadronic interactions result in the production of energetic photons mostly from the decay of neutral pions: we follow [17] for the computation of the gamma-ray emission emerging from each paired cloud. A list of the ten most promising illuminated clouds is provided in Tab. 1, where the main physical parameters of each cluster-cloud system are reported, particularly the cluster maximum energy, the distance of its center to the illuminated cloud (also in terms of the bubble
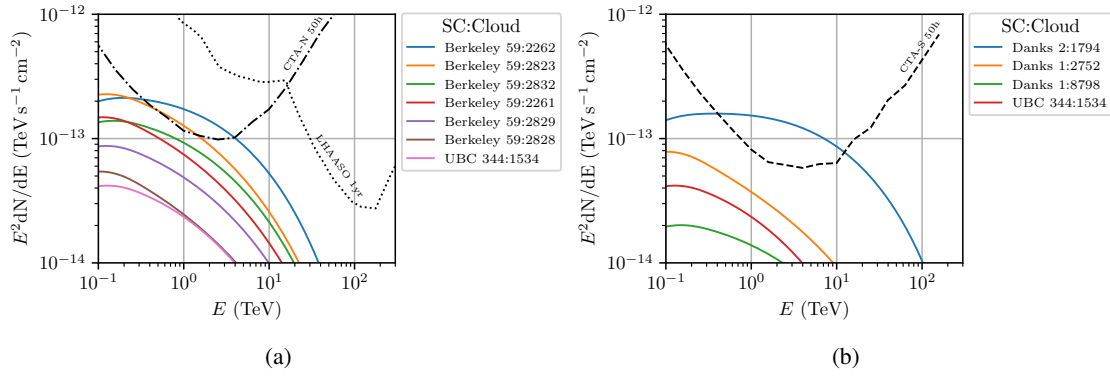
Figure 4: Gamma-ray energy-flux from detectable cluster-cloud pairings by (a) the Northern hemisphere detectors CTA-North (Alpha-array) and LHAASO, and (b) the Southern hemisphere detector CTA-South.

radius), as well as the cloud estimated mass and angular diameter, and its predicted integrated gamma-ray flux above 10 TeV, that includes both the contributions from the paired cluster and from the Galactic CR sea. Current gamma-ray flux upper limits are available from H.E.S.S. [18] and HAWC [19], none of which however violates the expected cloud fluxes according to the WTS model here presented. Next-generation instruments will be able to constrain our predictions at least for the most prominent clouds, as shown in Fig. 4, where cloud expected energy fluxes are compared to the CTA (alpha configuration) and LHAASO point-source differential sensitivities, taken respectively from [20] and [21]. This comparison indicates that a few illuminated clouds are possibly within the reach of CTA already with 50 hr of observations. However, one should consider that a degradation of performances is expected when observing extended sources, mostly because of the increased background rate involved in the analysis, as investigated in [22] for a different configuration of CTA telescopes adopted in the past. The molecular clouds under investigation are on average extended structures for both CTA and LHAASO, though the larger point spread function of the latter might mitigate the impact of sensitivity worsening. Detailed studies about detection prospects of both CTA and LHAASO with extended source sensitivities are currently in progress. Interestingly, 9 out of 10 among the brightest systems are illuminated by candidate PeVatron YMSCs, namely Danks 1, Danks 2, and Berkley 59, as it results from the model under investigation assuming Kraichnian-like diffusion coefficient. The reader is invited to look at [15] for a discussion about the gamma-ray emission expected from the clusters themselves.

5. Conclusions

The search for Galactic PeVatrons is witnessing a revolution with novel results from LHAASO [23]. Still, probing the nature of their radiative emission is not trivial and in this regard the presence of dense target gas nearby energetic accelerators constitutes ideal conditions for hadronic emission. We explore here the case of molecular clouds illuminated by protons accelerated at the WTS of YMSCs, considering the observed populations of both objects through the most sensitive surveys to date. We found that next generation instruments might probe the expected gamma-ray emission at least for some systems, thus shedding light on the PeV activity of the Milky Way SCs.

Cloud-ID	Cluster	$E_{\max}$ [PeV]	d [pc]	d/R_b	Cloud diameter [deg]	Cloud mass [M$_\odot$]	$F_\gamma^{\mathrm{cloud}}(>10\,\mathrm{TeV})$ [TeV cm^{-2} s^{-1}]
1794	Danks 2	5	59.9	0.33	0.73	3.2×10^4	1.06×10^{-13}
2262	Berkeley 59	1.3	29.6	0.29	1.18	1.1×10^4	4.32×10^{-14}
2823	Berkeley 59	1.3	71.7	0.70	1.41	1.8×10^4	2.05×10^{-14}
2832	Berkeley 59	1.3	54.8	0.53	0.97	8.2×10^3	1.69×10^{-14}
2261	Berkeley 59	1.3	80.6	0.78	1.14	1.2×10^4	1.17×10^{-14}
2752	Danks 1	3.1	106	0.94	0.90	2.6×10^4	9.03×10^{-15}
2829	Berkeley 59	1.3	71.6	0.70	0.77	6.1×10^3	7.86×10^{-15}
8798	Danks 1	3.1	81.2	0.72	0.31	2.5×10^3	4.14×10^{-15}
2828	Berkeley 59	1.3	88.8	0.86	0.82	5.9×10^3	3.87×10^{-15}
1534	UBC 344	0.9	87.5	0.55	0.90	3.6×10^4	3.33×10^{-15}

Table 1: Top 10 YMSC illuminated clouds. Columns are as follows: cloud ID from [10], cluster name from [8] and its predicted maximum energy as from the WTS model here presented, absolute distance among cluster and cloud centers, ratio among cloud distance and cluster bubble radius, cloud angular diameter and estimated mass, and expected integral (above 10 TeV) gamma-ray flux from the illuminated cloud.

6. Acknowledgments

References

[1] M. Casse & J. A. Paul, *ApJ*, **258** (1982) 860C;
[2] F. Aharonian, R. Yang & E. de Ona Wilhelmi, *Nature Astronomy* **3** (2019) 561;
[3] Z. Cao et al. [LHAASO Coll.], Nature **594** (2021) 33;
[4] G. Morlino, P. Blasi, E. Peretti & P. Cristofari, *MNRAS* **504** (2021) 6069;
[5] S. Gupta, B. B. Nath, P. Sharma & D. Eichler, *MNRAS* **493** (2020) 3159;
[6] D. V. Badmaev, A. M. Bykov & M. E. Kalyashova, *MNRAS* **517** (2022) 2818;
[7] T. Vieu & B. Reville, *MNRAS* **519** (2023) 136;
[8] T. Cantat-Gaudin et al. [Gaia Coll.], *A&A* **640** (2020) A1;
[9] S. Gabici, F. Aharonian & S. Casanova, *MNRAS* **396** (2009) 1629;
[10] A. Mitchell, G. Rowell, S. Celli & S. Einecke, *MNRAS* **503** (2021) 3;
[11] M. A. Miville-Deschenes, N. Murray & E. J. Lee, *ApJ* **834** (2017) 57;
[12] R. Weaver, R. McCray, Castor, P. Shapiro & R. Moore, *ApJ* **218** (1977) 377;
[13] R. Kharchenko, A. E. Piskunov, E. Schilbach, S. Roser & R. D. Scholz, *A&A* **558** (2013) A53;
[14] T. Vieu, S. Gabici, V. Tatischeff & S. Ravikularaman, *MNRAS* **512** (2022) 1275;
[15] C. Weidner & P. Kroupa, *MNRAS* **348** (2004) 178;
[16] A. Mitchell et al., PoS(ICRC2023) **611** (2023);
[17] T. M. Dame, D. Hartmann & P. Thaddeus, *ApJ* **547** (2001) 792;
[18] S. R. Kelner, F. Aharonian, & V. V. Bugayov, *Phys. Rev. D* **74** (2006) 034018
[19] H. Abdalla et al. [H.E.S.S. Collaboration], *A&A* **612** (2018) A1;
[20] A. Albert et al. [HAWC Collaboration], *ApJ* **905** (2020) 76A;
[21] CTA Observatory and Consortium, Zenodo (2021) 10.5281/zenodo.5499840;
[22] X. Y. Wang et al. [LHAASO Collaboration], *Chinese Physics C* **46** (2022) 3;
[23] L. Ambrogi, S. Celli & F. Aharonian, *Astroparticle Physics* **100** (2018) 69A;
[24] C. Zhen et al. [LHAASO Collaboration], arXiv:2305.17030.